Journal of Electroanalytical Chemistry 684 (2012) 32–37

Contents lists available at SciVerse ScienceDirect

Journal of Electroanalytical Chemistry

journal homepage: www.elsevier.com/locate/jelechem

Short communication

Compressible aligned carbon nanotube/MnO_2 as high-rate electrode materials for supercapacitors

Ying Xiao [a], Qiang Zhang [b], Jun Yan [a], Tong Wei [a], Zhuangjun Fan [a,*], Fei Wei [b]

[a] Key Laboratory of Superlight Materials and Surface Technology, Ministry of Education, College of Material Science and Chemical Engineering, Harbin Engineering University, Harbin 150001, China
[b] Beijing Key Laboratory of Green Chemical Reaction Engineering and Technology, Department of Chemical Engineering, Tsinghua University, Beijing 100084, China

ARTICLE INFO

Article history:
Received 10 April 2012
Received in revised form 15 August 2012
Accepted 26 August 2012
Available online 04 September 2012

Keywords:
Aligned carbon nanotube
MnO_2
Electrochemical properties

ABSTRACT

Aligned carbon nanotube (ACNT)/MnO_2 nanocomposites were fabricated using the reduction between potassium permanganate and ACNT under the microwave irradiation. Due to good contact between ACNT and current collector during the charge/discharge process, compressible ACNT/MnO_2 nanocomposites show better electrochemical properties compared to pure MnO_2 and ACNT, such as high specific capacitance, good rate performance and cycling stability (2.7% loss of the initial value after 3000 cycles). These results demonstrate that ACNT/MnO_2 nanocomposites have potential application for supercapacitors as high-rate electrode materials.

1. Introduction

Recently, supercapacitor has become one of the most promising energy storage devices due to the increasing power demand for portable devices and automotive applications [1]. Based on different energy storage mechanisms [2–4], pseudo-capacitor possessing both double-layers effects and Faradaic reactions shows higher energy density than electrical double-layer capacitor (EDLC) [2–5]. Among pseudocapacitive transition-metal oxides such as RuO_2, NiO, and MnO_2 [6–8], manganese oxide has recently received considerable attention as electrode material for supercapacitors due to its high theoretical specific capacitance (1110 F g^{-1}) [9], low cost, and environmental friendly characteristics [10,11]. Up to now, nanostructured manganese oxides possessing high specific surface area and short proton-transport path can effectively improve their specific capacitance [12–19]. However, the poor conductivity of MnO_2 (10^{-5}–10^{-6} S cm^{-1}) results in low rate capability for high power performance, thus limiting its wide application in energy storage systems [20]. To improve the electrical conductivity of MnO_2 electrode materials, the combination of highly conductive materials such as carbon nanotubes (CNTs) [21–25], graphene [26,27], or conducting polymers [28,29], as a hybrid structure, has been explored to improve the electrochemical performance.

During the past 20 years, random CNTs as electrode materials have been widely investigated for energy applications, such as supercapacitor [30–41], Li-ion batteries [42–46], and fuel cell [47]. Whereas aligned CNTs with supercompressible response, excellent strength and flexibility under mechanical compression can be used as nano- and microscale springs or shock absorbers [48]. However, the use of vertically aligned CNTs (ACNT) as electrode materials is rarely reported. Recently, the incorporation of MnO_2 with ACNT grown on the Ta foils exhibits good rate capability and high capacitance [49]. However, such a thin film limits its further practical application. As we have demonstrated previously, nanostructured MnO_2 anchored on the surfaces of random CNTs synthesized by the reduction of potassium permanganate under microwave irradiation, exhibits high capacitance and excellent cycle stability [25].

In this paper, we used the reaction between potassium permanganate and ACNTs under microwave irradiation to prepare the ACNT/MnO_2 nanocomposites as electrode materials for supercapacitors (Fig. 1). Nanoscale MnO_2 particles uniformly deposit on the surface of compressible spring-like ACNTs, which recover themselves during the charge/discharge process to maintain good contact with current collector due to their excellent mechanical strength and compressibility [50,51]. Therefore, ACNT/MnO_2 nanocomposites show good rate performance, meaning that ACNT played an important role in the ion and electron transport during the electrochemical reaction.

2. Experimental

2.1. Synthesis of ACNTs and ACNT/MnO_2 nanocomposites

ACNTs were synthesized according to the previous report [51]. Briefly, Fe/Mo/vermiculite was placed into a quartz tube, main-

* Corresponding author. Tel./fax: +86 451 82569890.
E-mail address: fanzhj666@163.com (Z. Fan).

1572-6657/$ - see front matter © 2012 Elsevier B.V. All rights reserved.
http://dx.doi.org/10.1016/j.jelechem.2012.08.024

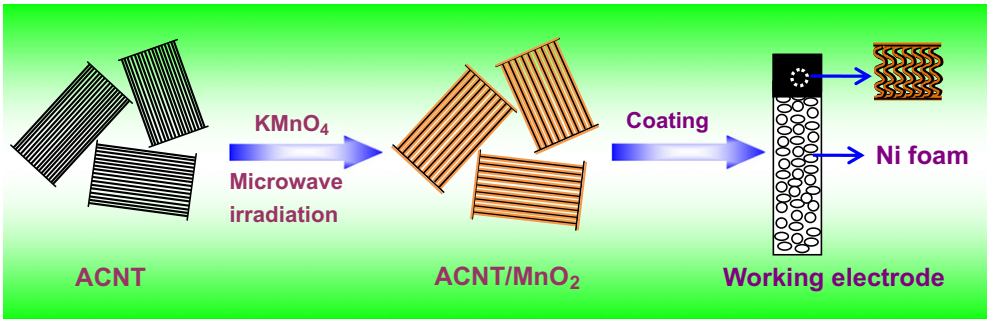

Fig. 1. Schematic illustration of the synthesis of ACNT/MnO_2 composite as electrode material.

tained at 650 °C within an atmosphere of argon and hydrogen (10:1) at a flow rate of 600 mL min^{-1}. Then, a mixture of ethylene (80 mL min^{-1}), argon (550 mL min^{-1}) and hydrogen (50 mL min^{-1}) was introduced into the quartz tube for 15 min to allow CNT growth. ACNT/MnO_2 nanocomposites were prepared as follows: At first, 0.2 g ACNT was added into 100 mL distilled water and stirred for 3 h. Then predetermined amount of $KMnO_4$ (ACNT and $KMnO_4$ mass ratio of 1:1, 3:7, 7:3, respectively) was added into the above suspension and stirred for 1 h, subsequently heated using a household microwave oven (Haier MA-2270, 2450 MHz, 700 W) for 5 min. Finally, the suspension was filtered, washed several times with distilled water and absolute alcohol, and dried in an oven at 100 °C for 12 h. The resulting black powder was collected for the following characterization. For comparison, birnessite-type MnO_2 was also synthesized under hydrothermal condition as described elsewhere [52].

2.2. Characterization

The samples were analyzed by a powder X-ray diffraction system (XRD, TTR-III) equipped with Cu Kα radiation ($\lambda = 0.15406$ nm). The microstructure of the samples was optically studied by a scanning electron microscopy (SEM, Camscan Mx2600FE) and transition electron microscopy (TEM, JEOL JEM2000FX).

2.3. Electrochemical measurements

As-prepared nanocomposites, carbon black and poly(tetrafluoroethylene) (PTFE) were dispersed in ethanol, and their mass ratio was 75:20:5. Then the mixture was coated onto nickel foam (1×1 cm^2) with a spatula, which was followed by drying at 100 °C for 12 h in a vacuum oven.

All electrochemical measurements were done in a three electrode setup: A Ni foam coated with as-prepared nanocomposites as the working electrode, a platinum foil as the counter electrode, and a saturated calomel electrode (SCE) as the reference electrode. The electrochemical measurements included cyclic voltammograms (CVs), galvanostatic charge/discharge and electrochemical impedance spectroscopy (EIS), which were measured by a CHI 660C electrochemical workstation. All electrochemical measurements were carried out in a 1 mol L^{-1} Na_2SO_4 aqueous electrolyte at room temperature and the potential range was −0.1 to 0.9 V (vs. SCE).

3. Results and discussion

3.1. Microstructure characterization

The typical XRD patterns of ACNT, pure MnO_2 and ACNT/48%-MnO_2 are shown in Fig. 2. The presence of birnessite-type MnO_2 (JCPDS 42-1317) with mixed crystalline and amorphous parts was confirmed by the XRD analysis. Three broad peaks at 2θ around 12°, 37° and 66° can be indexed to brinessite-type MnO_2 [53,54]. Broad peaks correspond to poorly crystallized compound indicate amorphous nature of the powder.

The morphology of ACNTs shows stacking structure with a length of 5–20 μm as shown in Fig. 3a. After MnO_2 deposition, the stacking structure of ACNTs still keeps its morphology (Fig. 3b and c). In this work, the self-limiting reaction between permanganate and carbon was applied to deposit birnessite MnO_2 onto the surface of ACNT (the diameter of 10–20 nm, Fig. 3d). Therefore, the advantage of this process is that thin MnO_2 film closely anchored on the surface of nanotubes (Fig. 3e). For comparison, pure MnO_2 with flower-like structure was also prepared by the hydrothermal synthesis method (Fig. 3f).

3.2. Electrochemical behavior of the ACNT/MnO_2 electrodes

Fig. 4a shows the CV curves of ACNT and ACNT/MnO_2 nanocomposites at the same scan rate of 20 mV s^{-1}. CV curve of ACN is relatively rectangular in shape, indicating an ideal capacitive behavior. With the MnO_2 loading increasing from 25 to 64 wt.%, CV curves of the ACNT/MnO_2 electrodes are still symmetrical.

The specific capacitance of the electrode can be calculated according to the following equation:

$$C = \left(\int I\,dV\right)/(\upsilon m V) \quad (1)$$

where I is the response current density (A cm^{-2}), V is the potential (V), υ is the potential scan rate (mV s^{-1}), and m is the mass of the electroactive materials in the electrodes (g).

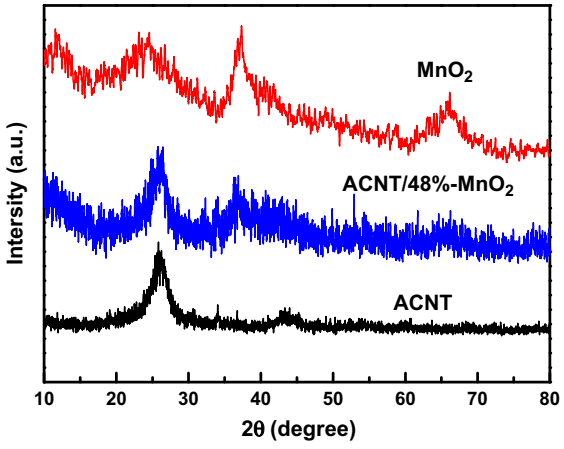

Fig. 2. Typical XRD patterns of ACNT, pure MnO_2 and ACNT/48%-MnO_2 composite.

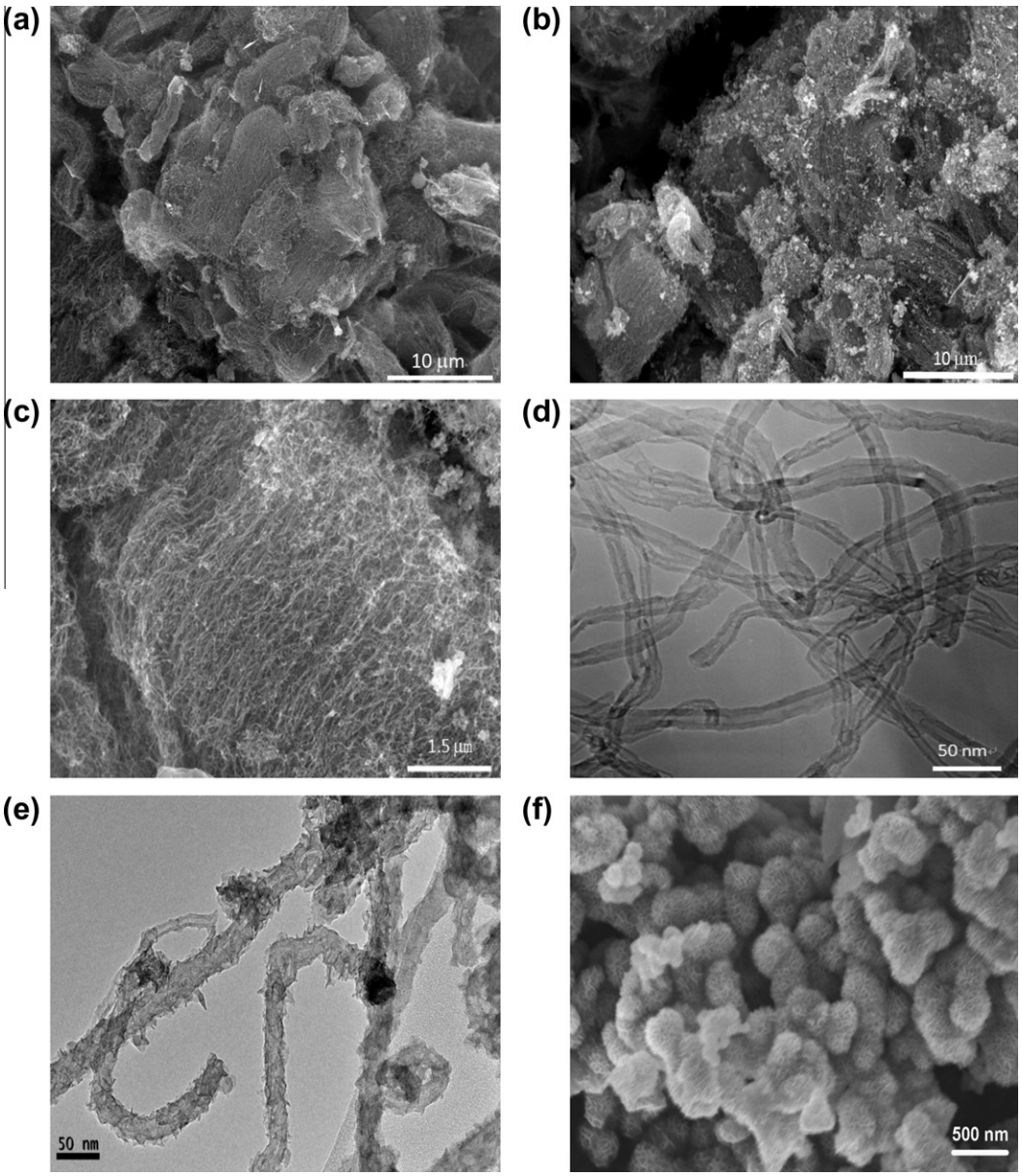

Fig. 3. SEM images of ACNT (a) and ACNT/48%-MnO_2 (b and c). TEM image of ACNT (d) and ACNT/48%-MnO_2 (e). SEM image of pure MnO_2 exhibiting flower-like structure (f).

Fig. 4b shows that the discharge time for ACNT/48%-MnO_2 is about six times higher than that of ACNT at the same current density of 5 A g^{-1}, meaning high energy storage after MnO_2 loading onto ACNT. Moreover, the linear voltage–time profile and the highly symmetric charge/discharge characteristics show good capacitive behavior. The ACNT/MnO_2 nanocomposite electrodes exhibit an enhanced capacitance performance and rate capability compared with ACNT electrode (Fig. 4c). For ACNT electrode, its specific capacitance is only 40.6 F g^{-1} at 5 mV s^{-1}, while all ACNT/MnO_2 electrodes show high specific capacitance and good capacitance retention. For example, the specific capacitance of ACNT/48%-MnO_2 is 194.5 F g^{-1} at 5 mV s^{-1} and 165.4 F g^{-1} at 200 mV s^{-1}, meaning a high-rate electrode for supercapacitor. When MnO_2 loading is increased to 64 wt.%, there is a decrease in specific capacitance due to dense or agglomerate MnO_2 with limited electrochemically active surface area [55].

The cycling stabilities of ACNT and ACNT/48%-MnO_2 nanocomposite electrode were measured by CVs at 100 mV s^{-1} in 1 M Na_2SO_4 solution. It is obviously observed that the specific capacitance of ACNT/48%-MnO_2 is much higher than that of ACNT, only 2.7% capacitance loss after 3000 cycles. The good cycling stability of the ACNT/48%-MnO_2 composite electrode can be explained by the following reasons: On the one hand, compressible ACNT can effectively inhibit the conductivity loss due to the volume change of electrode material during the repeat CV cycles. On the other hand, the stacking structure of ACNT is beneficial to the ion transport from the electrolyte solution to the surface of the MnO_2.

Moreover, pure MnO_2 as electrode material was also investigated for comparison. CV curves of MnO_2 and ACNT/48%-MnO_2 nanocomposite at 20 mV s^{-1} in 1 M Na_2SO_4 solution are shown in Fig. 5a. Compared to pure MnO_2, CV curve of ACNT/48%-MnO_2 is relatively rectangular in shape and exhibits near mirror-image current response on voltage reversal, meaning ideal capacitive behavior. At the same time, the galvanostatic charge/discharge curves of the ACNT/48%-MnO_2 nanocomposite

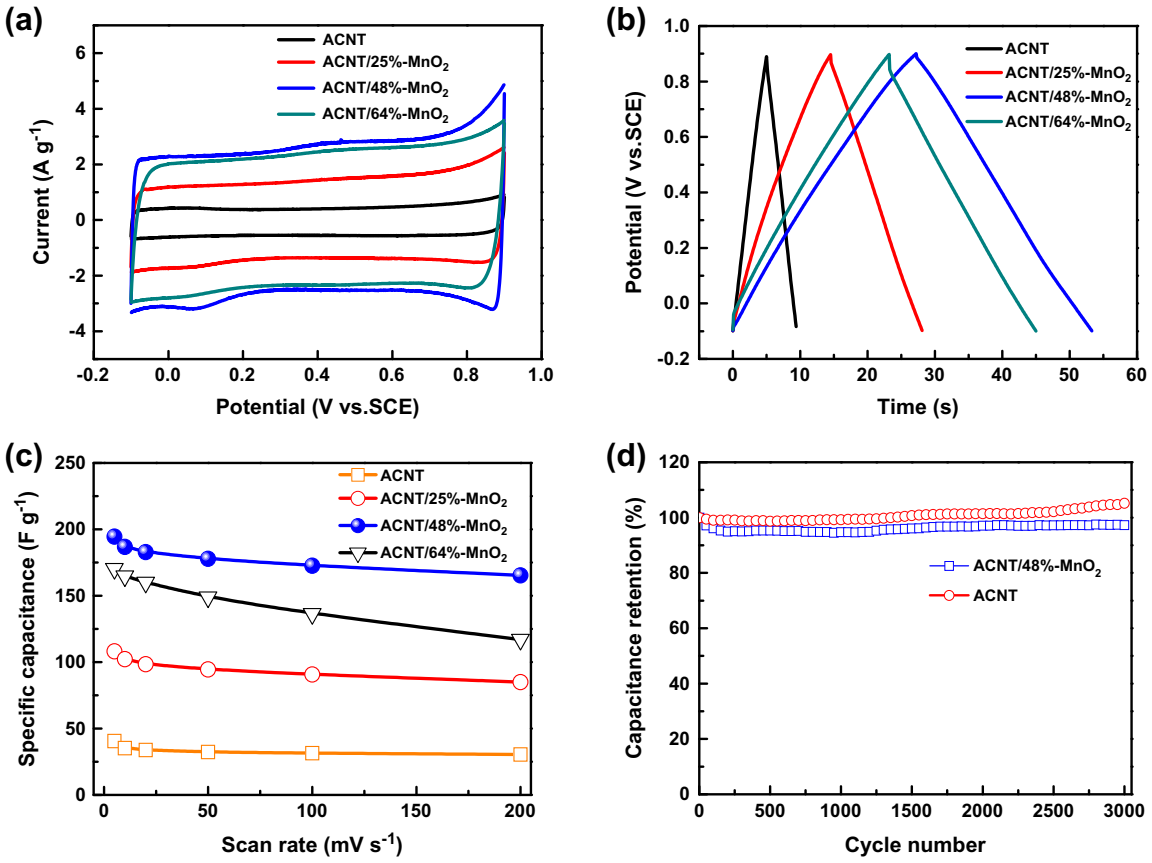

Fig. 4. (a) CV curves of ACNT and ACNT/MnO_2 nanocomposite at 20 mV s^{-1} in 1 M Na_2SO_4 solution. (b) Galvanostatic charge/discharge curves of ACNT and ACNT/MnO_2 nanocomposite at a current density of 5 A g^{-1}. (c) Specific capacitances of ACNT and ACNT/MnO_2 nanocomposite at different scan rates. (d) Cycle stability of ACNT and ACNT/48%-MnO_2 at 100 mV s^{-1} in 1 M Na_2SO_4 solution.

(Fig. 5b) are highly linear and symmetrical. In addition, the cure of ACNT/48%-MnO_2 has little *iR* drop (0.01 V) compared with pure MnO_2 (0.06 V), indicating a rapid *I–V* response and an excellent electrochemical reversibility.

There are two mechanisms proposed for the charge storage in MnO_2 material. The first one is based on the concept of H^+ or alkali metal cations (C^+) such as Na^+ in this case during reduction and deintercalation upon oxidation. This process is accompanied by the reversible reaction of Mn^{4+}/Mn^{3+}.

$$MnO_2 + C^+ + e^- \leftrightarrow MnOOC \quad (2)$$

The second one is the adsorption of cations present in the electrolyte on the MnO_2 surface.

$$(MnO_2)_{surface} + C^+ + e^- \leftrightarrow (MnO_2{-}C^+)_{surface} \quad (3)$$

For hydrous MnO_2, a common viewpoint is that the redox process is mainly governed by the insertion and deinsertion of Na+ and or H+ from the electrolyte into the nanostructured MnO_2 matrix [56,57]. Increasing the scanning rate will have a direct impact on the diffusion time of cations into the matrix leading to the sharp decrease of available capacity [58].

ACNT/48%-MnO_2 nanocomposite exhibits higher specific capacitance from 5 to 200 mV s^{-1} (Fig. 5c), compared with pure MnO_2 (172.2 F g^{-1} at 5 mV s^{-1} and 93.6 F g^{-1} at 200 mV s^{-1}). In addition, the capacitance of ACNT/48%-MnO_2 at 10 mV s^{-1} is lower than that of random CNT/48%-MnO_2 based on the overall electroactive material, however, ACNT/48%-MnO_2 exhibits the best rate performance than pure MnO_2 and random CNT/48%-MnO_2 due to its stacking structure (Fig. 5d). The improved electrochemical performance was also confirmed by Electrochemical Impedance Spectroscopy, which is presented in Fig. 5e. It can be seen that the impedance spectra are almost similar in form, composed of one semicircle at high-frequency end followed by a linear part at the low-frequency end. The spectra of ACNT/48%-MnO_2 show nearly 90° capacitive spike starting from the mid-high frequency, indicating the suitability of ACNT/48%-MnO_2 composite as an electrode material for supercapacitors. In addition, the equivalent series resistances (ESR) for ACNT/48%-MnO_2 electrode extracted from 100 kHz is estimated to be ~0.39 Ω, in contrast to ~0.60 Ω for MnO_2 electrode, meaning higher conductivity and more capacitive behavior of electrode for supercapacitors.

4. Conclusions

In summary, ACNT/MnO_2 nanocomposites were synthesized using the reduction between potassium permanganate and ACNT under microwave irradiation. ACNT/48%-MnO_2 as electrode materials show excellent electrochemical properties, such as good rate performance, and excellent cycle stability (only 2.7% capacitance loss after 3000 cycles). Compared with random CNT, the integration of ACNT and MnO_2 enables such nanocomposite to possess better rate performance due to the excellent compression and resilience properties of ACNT. Meanwhile, the stacking structure of ACNT also improves the diffusion of electrolyte ions in the electrode. Therefore, such kind of nanocomposite would be a promising high-rate electrode material for supercapacitor.

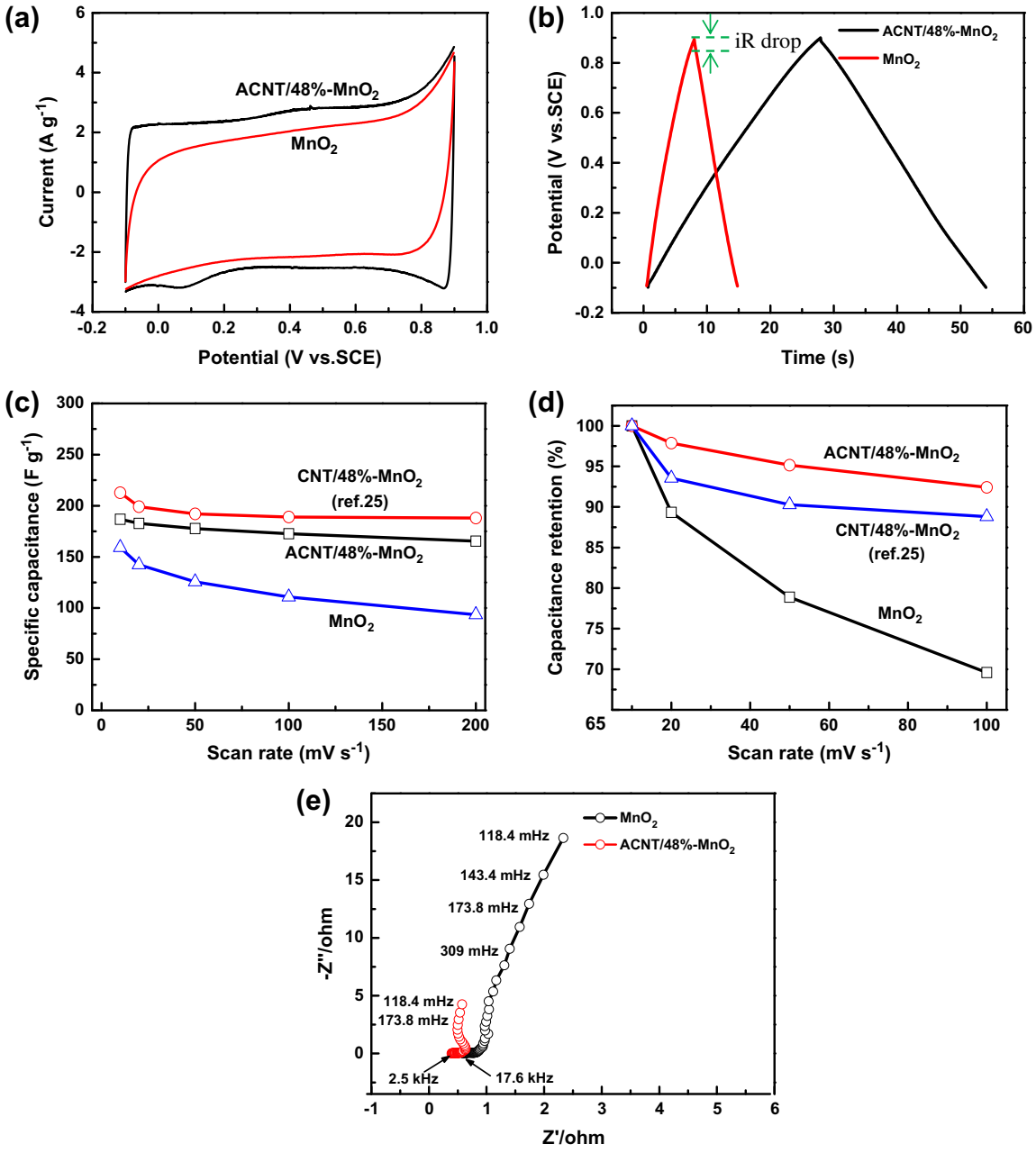

Fig. 5. (a) CV curves of pure MnO_2 and ACNT/48%-MnO_2 nanocomposite at 20 mV s^{-1} in 1 M Na_2SO_4 aqueous solution. (b) Galvanostatic charge/discharge curves of pure MnO_2 and ACNT/48%-MnO_2 nanocomposite at 5 A g^{-1}. (c) Specific capacitance of pure MnO_2, ACNT/48%-MnO_2 and CNT/48%-MnO_2 nanocomposite at different scan rates. (d) Capacitance retention of pure MnO_2, ACNT/48%-MnO_2 and CNT/48%-MnO_2 nanocomposite at different scan rates. (e) Nyquist plots of MnO_2 and ACNT/48%-MnO_2 electrode in the frequency range of 100 kHz to 0.1 Hz.

Acknowledgements

The authors acknowledge financial supports from the National Science Foundation of China (51077014, 21003028), Fundamental Research Funds for the Central Universities and Program for New Century Excellent Talents in University (NCET-10-0050).

References

[1] C.L. Ho, M.S. Wu, J. Phys. Chem. C. 115 (2011) 22068–22074.
[2] B.E. Conway, Electrochemical Supercapacitors: Scientific Fundamentals and Technological Applications, Kluwer Academic/Plenum, New York, 1999.
[3] P. Simon, Y. Gogotsi, Nat. Mater. 7 (2008) 845–854.
[4] A.S. Arico, P. Bruce, B. Scrosati, J.M. Tarascon, W. VanSchalkwijk, Nat. Mater. 4 (2005) 366–377.
[5] M. Winter, R. Brodd, J. Chem. Rev. 105 (2005) 1021–11021.
[6] T. Cottineau, M. Toupin, T. Delahaye, T. Brousse, D. Belanger, Appl. Phys. A: Mater. Sci. Process. 82 (2006) 599–606.
[7] M. Toupin, T. Brousse, D. Belanger, Chem. Mater. 16 (2004) 3184–3190.
[8] D.W. Wang, F. Li, H.M. Cheng, J. Power Sources 185 (2008) 1563–1568.
[9] S.C. Pang, M.A. Anderson, T.W.J. Chapman, Electrochem. Soc. 147 (2000) 444–450.
[10] H.Y. Lee, J.B. Goodenough, J. Solid State Chem. 144 (1999) 220–223.
[11] W.F. Wei, X.W. Cui, W.X. Chen, D.G. Ivey, Chem. Soc. Rev. 40 (2011) 1697–1721.
[12] J.K. Yuan, W.N. Li, S. Gomez, S.L. Suib, J. Am. Chem. Soc. 127 (2005) 14184–14185.
[13] M. Yin, S. O'Brien, J. Am. Chem. Soc. 125 (2003) 10180–10181.
[14] X.H. Zhong, R.G. Xie, R.G. Sun, I. Lieberwirth, W. Knoll, J. Phys. Chem. B. 110 (2006) 2–4.
[15] L.C. Zhang, Z.H. Liu, H. Lv, X.H. Tang, K. Ooi, J. Phys. Chem. C. 111 (2007) 8418–8423.
[16] M.S. Wu, P.J. Chiang, J.T. Lee, J.C. Lin, J. Phys. Chem. B. 109 (2005) 23279–23284.
[17] F.Y. Cheng, J. Chen, X.L. Gou, P.W. Shen, Adv. Mater. 17 (2005) 2753–2756.

[18] V. Subramanian, H.W. Zhu, R. Vajtai, P.M. Ajayan, B.Q. Wei, J. Phys. Chem. B. 109 (2005) 20207–20214.
[19] Y. Oaki, H. Imai, Angew. Chem. Int. Ed. 46 (2007) 4951–4955.
[20] D. Belanger, T. Brousse, J.W. Long, Electrochem. Soc. Interfaces 17 (2008) 49–52.
[21] S.B. Ma, K.W. Nam, W.S. Yoon, X.Q. Yang, K.Y. Ahn, K.H. Oh, K.B. Kim, J. Power Sources 178 (2008) 483–489.
[22] S.R. Sivakkumar, J.M. Ko, D.Y. Kim, B.C. Kim, G.G. Wallace, Electrochim. Acta 52 (2007) 7377–7385.
[23] S.W. Lee, J. Kim, S. Chen, P.T. Hammond, Y. Shao-Horn, ACS Nano 4 (2010) 3889–3896.
[24] L. Hu, M. Pasta, F.L. Mantia, L. Cui, S. Jeong, H.D. Deshazer, J.W. Choi, S.M. Han, Y. Cui, Nano Lett. 10 (2010) 708–714.
[25] J. Yan, Z. Fan, T. Wei, J. Cheng, B. Shao, K. Wang, P. Song, M. Zhang, J. Power Sources 194 (2009) 1202–1207.
[26] J. Yan, Z. Fan, T. Wei, W. Qian, M. Zhang, F. Wei, Carbon 48 (2010) 3825–3833.
[27] G. Yu, L. Hu, M. Vosgueritchian, H. Wang, X. Xie, J.R. McDonough, X. Cui, Y. Cui, Z. Bao, Nano Lett. 11 (2011) 2905–2911.
[28] R. Liu, S.B. Lee, J. Am. Chem. Soc. 130 (2008) 2942–2943.
[29] L. Chen, L.J. Sun, F. Luan, Y. Liang, Y. Li, X.X. Liu, J. Power Sources 195 (2010) 3742–3747.
[30] K.H. An, W.S. Kim, Y.S. Park, Y.C. Choi, S.M. Lee, D.C. Chung, D.J. Bae, S.C. Lim, Y.H. Lee, Adv. Mater. 13 (2001) 497–500.
[31] M. Hughes, M.S.P. Shaffer, A.C. Renouf, C. Singh, G.Z. Chen, J. Fray, A.H. Windle, Adv. Mater. 14 (2002) 382–385.
[32] M. Hughes, G.Z. Chen, M.S.P. Shaffer, D.J. Fray, A.H. Windle, Chem. Mater. 14 (2002) 1610–1613.
[33] K.H. An, W.S. Kim, Y.S. Park, J.M. Moon, D.J. Bae, S.C. Lim, Y.S. Lee, Y.H. Lee, Adv. Funct. Mater. 11 (2001) 387–392.
[34] C.Y. Liu, A.J. Bard, F. Wudl, I. Weitz, J.R. Heath, Electrochem. Solid State Lett. 2 (1999) 577–578.
[35] J.N. Barisci, G.G. Wallace, R.H. Baughman, J. Electroanal. Chem. 488 (2000) 92–98.
[36] L. Diederich, E. Barborini, P. Piseri, A. Podesta, P. Milani, A. Schneuwly, R. Gallay, Appl. Phys. Lett. 75 (1999) 2662–2664.
[37] E. Frackowiak, K. Metenier, V. Bertagna, F. Beguin, Appl. Phys. Lett. 77 (2000) 2421–2423.
[38] E. Frackowiak, K. Jurewicz, S. Delpeux, F. Beguin, J. Power Sources 97–98 (2001) 822–825.
[39] B.J. Yoon, S.H. Jeong, K.H. Lee, H.S. Kim, C.G. Park, J.H. Han, Chem. Phys. Lett. 388 (2004) 170–174.
[40] E. Frackowiak, K. Jurewicz, K. Szostak, S. Delpeux, F. Beguin, Fuel Process. Technol. 77 (2002) 213–219.
[41] K.H. An, K.K. Jeon, J.K. Heo, S.C. Lim, D.J. Bae, Y.H. Lee, J. Electrochem. Soc. 149 (2002) A1058–A1062.
[42] A.S. Claye, J.E. Fischer, C.B. Huffman, A.G. Rinzler, R.E. Smalley, J. Electrochem. Soc. 147 (2000) 2845–2852.
[43] E. Frackowiak, S. Gautier, H. Gaucher, S. Bonnamy, F. Beguin, Carbon 37 (1999) 61–69.
[44] B. Gao, A. Kleinhammes, X.P. Tang, C. Bower, L. Fleming, Y. Wu, O. Zhou, Chem. Phys. Lett. 307 (1999) 153–157.
[45] H.C. Shin, M.L. Liu, B. Sadanadan, A.M. Rao, J. Power Sources 112 (2002) 216–221.
[46] G. Maurin, C. Bousquet, F. Henn, P. Bernier, R. Almairac, B. Simon, Chem. Phys. Lett. 312 (1999) 14–18.
[47] C. Nutzenadel, A. Zuttel, D. Chartouni, L. Schlapbach, Electrochem. Solid State Lett. 2 (1999) 30–32.
[48] A. Cao, P.L. Dickrell, W.G. Sawyer, M.N. Ghasemi-Nejhad, P.M. Ajayan, Science 310 (2005) 1307–1310.
[49] H. Zhang, G. Cao, Z. Wang, Y. Yang, Z. Shi, Z. Gu, Nano Lett. 8 (2008) 2664–2668.
[50] Z.J. Fan, J. Yan, G.Q. Ning, T. Wei, W.Z. Qian, S.J. Zhang, Q. Zhang, F Wei, Carbon 48 (2010) 4197–4214.
[51] Q. Zhang, M.Q. Zhao, Y. L, Y. Liu, A.Y. Cao, W.Z. Qian, Y.F. Lu, F. Wei, Adv. Mater. 21 (2009) 2876–2880.
[52] J. Yan, T. Wei, J. Cheng, Z. Fan, M. Zhang, Mater. Res. Bull. 45 (2010) 210–215.
[53] S.B. Ma, K.Y. Ahn, E.S. Lee, K.H. Oh, K.B. Kim, Carbon 45 (2007) 375–382.
[54] X. Jin, W. Zhou, S. Zhang, G.Z. Chen, Small 3 (2007) 1513–1517.
[55] D. Belanger, T. Brousse, J.W. Long, Electrochem. Soc. Interfaces 17 (2008) 49–52.
[56] T. Brousse, M. Toupin, R. Dugas, L. Athouël, O. Crosnier, D. Ɓelanger, J. Electrochem. Soc. 153 (2006) A2171–A2180.
[57] V. Subramanian, H.W. Zhu, B.Q. Wei, J. Power Sources 159 (2006) 361–364.
[58] C. Xu, B. Li, H. Du, F. Kang, Y. Zeng, J. Power Sources 180 (2008) 664–670.